Available online at www.sciencedirect.com

SciVerse ScienceDirect

Ceramics International 38 (2012) 5813–5820

CERAMICS INTERNATIONAL

www.elsevier.com/locate/ceramint

Effects of heat treatment conditions on the structural and magnetic properties of MgCuZn nano ferrite

Ch. Sujatha [a,*], K. Venugopal Reddy [a], K. Sowri Babu [a], A. RamaChandra Reddy [a], K.H. Rao [b]

[a] Department of Physics, National Institute of Technology Warangal, 506004, Andhra Pradesh, India
[b] Department of Physics, RGU-IIIT Nuzvid, Nuzvid 521201, Andhra Pradesh, India

Received 16 March 2012; received in revised form 9 April 2012; accepted 9 April 2012
Available online 19 April 2012

Abstract

$Mg_{0.5}Cu_{0.05}Zn_{0.45}Fe_2O_4$ nanoparticles were prepared through sol–gel method using polyvinyl alcohol as a chelating agent. The as prepared sample was annealed at three different temperatures (500 °C, 700 °C and 900 °C). The phase formation, morphology and magnetic properties with respect to annealing temperature were studied using the characterisation techniques like X-ray diffraction (XRD) as well as Fourier transform infrared spectroscopy (FTIR), field emission scanning electron microscopy (FESEM) and vibrating sample magnetometer (VSM), respectively. The crystallite size and magnetisation showed increasing trend with annealing temperature. The coercivity increased up to a particular annealing temperature and decreased thereafter, indicating transition from single domain to multi domain state with increasing annealing temperature. Further, to know the suitability of the material, as a ferrite core, in multilayer chip inductors, the powder sample annealed at 500 °C was compacted in the form of torroids and sintered at three different temperatures (800 °C, 900 °C and 950 °C). The permeability showed increasing trend with the increase of sintering temperature since the permeability depends on microstructure. The frequency dispersion of permeability, for the sintered samples, demonstrated high frequency stability as well as high operating frequency. The cut-off frequency for the sintered samples 800 °C, 900 °C and 950 °C is 32 MHz, 30.8 MHz and 30.4 MHz, respectively.

Keywords: A. Sol–gel processes; A. Sintering; C. Magnetic properties; D. Spinels; Permeability

1. Introduction

The synthesis of spinel ferrite nanoparticles has been intensively studied in recent years due to their potential applications in high-density magnetic recording, micro-wave devices and magnetic fluids [1]. These materials are considered superior to other magnetic materials because of low eddy current losses due to high electrical resistivity. The high frequency electromagnetic devices like microwave absorbers, converters and inductors require high initial permeability at radio frequency range [2]. Recently there is a growing interest on MgZn ferrites for electronic device applications instead of NiZn ferrites since nickel and its compounds produces carcinogenic effects and environmental toxicity, despite of their high permeability and high resistivity at higher frequencies [3]. There are several reports existed in the literature on NiCuZn ferrite system having good electromagnetic properties with low sintering temperature. These materials found to be appropriate for multilayer chip inductor applications (MLCIs) [4,5]. But unfortunately, these ferrites are sensitive to stress which adversely affect the inductance and hence the magnetic properties of the material. This is due to high magnetostriction constant of NiCuZn ferrite [6]. The main requirement of MLCIs materials are high permeability at higher frequency; good frequency stability over a large frequency band width along with low sintering temperature. Thus in search for an alternate material for MLCIs, MgCuZn ferrite was chosen since it has high electrical resistivity:high Curie temperature:good environmental stability and that too they are available at low cost [7]. Besides that MgCuZn ferrite has low magnetostriction constant than NiCuZn ferrite [8]. Nowadays, attention is being paid towards MgZn ferrite (superparamagnetic particles) for the treatment of magnetic hyperthermia [9]. Also the mixed spinels of the type

* Corresponding author. Tel.: +91 870 2462560; fax: +91 870 2459547; Mobile: +91 09502899683.
E-mail address: sujatha.phys09@gmail.com (Ch. Sujatha).

0272-8842/$36.00
http://dx.doi.org/10.1016/j.ceramint.2012.04.029

$Mg_{1-x}Zn_xFe_2O_4$ have weaker exchange coupling among A and B sites thereby reducing anisotropy constant. Hence there is a possibility of existence of superparamagnetic relaxation at room temperature even for big sized particles in such type of compositions [10].

Yue et al. [11] investigated $(Mg_{0.5-x}Cu_xZn_{0.5})O(Fe_2O_3)_{0.98}$ ferrite system and observed an improved permeability with Cu substitution but the critical frequency was around 10 MHz. Barati [12] studied electromagnetic properties of $Mg_{0.8-x}Cu_{0.2}Zn_xFe_2O_4$ ferrite prepared through nitrate–citrate auto combustion method .The results showed an improved permeability as the Zn content increases, but with poor frequency stability (2 MHz). Manjurul Haque et al. [13] investigated magnetic and dielectric behaviour of $Mg_{0.55-x}Cu_xZn_{0.45}O(Fe_2O_3)_{0.97}$ ($x = 0.0$–0.35) ferrite prepared through standard ceramic method which exhibited enhanced permeability with Cu substitution and the maximum relaxation frequency was around 5.7 MHz for $x = 0.2$. The literature reports on Cu substituted MgZn ferrites demonstrating high permeability but the relaxation frequencies are low in the order of few hundreds of kHz to MHz [11,13,14]. For improving the operating frequency of the MgCuZn ferrite material with low sintering temperature attempts were made.

Synthesis of nanoparticles having particle diameter smaller than the critical diameter is necessary for avoiding multi domain formation as well as hindering domain wall motion. In case of single domain particles, only contribution to magnetisation is by rotation of spin, thereby improving operating frequency of the material since spin rotation occurs in GHz frequency region. In the present work, $Mg_{0.5}Cu_{0.05}Zn_{0.45}Fe_2O_4$ nanoparticles were prepared through sol–gel method using polyvinyl alcohol as a chelating agent. The structural and magnetic properties of MgCuZn ferrite as a function of annealing temperature were investigated. This will provide information about the temperature required for formation of pure spinel phase and it is also useful to study the size dependent magnetic properties. The annealing temperature was chosen in such a way to obtain good magnetic properties as well as to attain low sintering temperature. Since fine particles are highly reactive and thereby reducing sintering temperature. In addition to that we have also studied frequency dispersion of permeability on the sintered samples at varied sintering temperatures. Since this will furnish magnitude of permeability and zone of utility of the material.

2. Experimental

$Mg_{0.5}Cu_{0.05}Zn_{0.45}Fe_2O_4$ ferrite nanoparticles were processed through sol–gel method. Analytical grade magnesium, zinc, copper and ferric nitrates were weighed in stoichiometric proportions and made them dissolved separately in deionised water. Thus obtained cationic solutions were mixed one into another and stirred continuously for one hour in order to improve homogeneity. To the resulting solution, precursor, polyvinyl alcohol (PVA) solution was added drop by drop under constant stirring and heating. The gelation continued step by step till a red gel type product was formed with the release of reddish brown gases at about 100 °C, leaving the fluffy mass in the reaction vessel. The as dried powder was annealed at three different temperatures 500 °C, 700 °C and 900 °C for 1 h. From hereafter, the three annealed samples were named as M5, M7 and M9. The sample annealed at low temperature (M5) was selected purposefully and compacted in the form of torroids using polyvinyl alcohol as a binder and sintered at three different temperatures 800 °C, 900 °C and 950 °C for 1 h with a heating rate of 5 °C/min in a programmable muffle furnace.

2.1. Characterization

The characterization of the prepared MgCuZn nanoparticles was conducted by various techniques to know the structure, particle size distribution and also to explore other properties of interest. The phase identification, crystallite size and lattice parameter were determined using X-ray diffraction (XRD) patterns collected from INEL XRG 3000 powder diffractometer with Co Kα radiation (λ = 1.78897 Å) in the 2θ range from 20° to 120°. Formation of spinel phase was also confirmed from Fourier transform infrared spectra (BRUKER OPTICS TENSOR 27) recorded in the wave number region 4000–400 cm^{-1} using KBr pellet method. The morphology and grain size distribution of nanoparticles having gold with palladium coated surfaces were investigated by field emission scanning electron microscope (FESEM) Carl Zeiss Ultra 55 operating at an accelerating high tension voltage EHT of 17 kV with a working distance WD of 8.5 mm, while the elemental analysis of the annealed samples were carried out using Energy Dispersive X-ray spectroscopy (EDS). Room temperature static magnetization measurements were carried out using vibrating sample magnetometer (EV-7 VSM) with a maximum applied field of 15 kOe. The frequency dispersion of permeability for the sintered samples was measured using High frequency LCR meter (WAYNKERR 6500P) in the frequency range from 100 Hz to 50 MHz.

3. Results and discussion

3.1. Structural analysis

X-ray diffraction patterns of both the annealed and sintered samples were shown in Fig. 1.The existence of highest intensity peak around the diffraction angle (2θ) equal to 41° for the samples corresponding to (3 1 1) plane, confirms the formation of spinel ferrite. In addition to that a broad peak at 2θ around 38° was noticed in the samples of M5 and M7 (indicated as star), corresponding to small trace of secondary phase (hematite α-Fe_2O_3). This is due to the fact that at low temperature, the atomic diffusion is slow thereby obstructing the formation of pure spinel phase of $Mg_{0.5}Cu_{0.05}Zn_{0.45}Fe_2O_4$ ferrite. In the case of sample M9, secondary phase is completely disappeared by forming pure spinel cubic phase. The peaks in the diffractograms were indexed by comparing observed interplanar distances (d) with standard JCPDS File No. 08-0234. The broad and well resolved peaks in the XRD patterns, for the samples M5 and M7 clearly demonstrated fine particles of

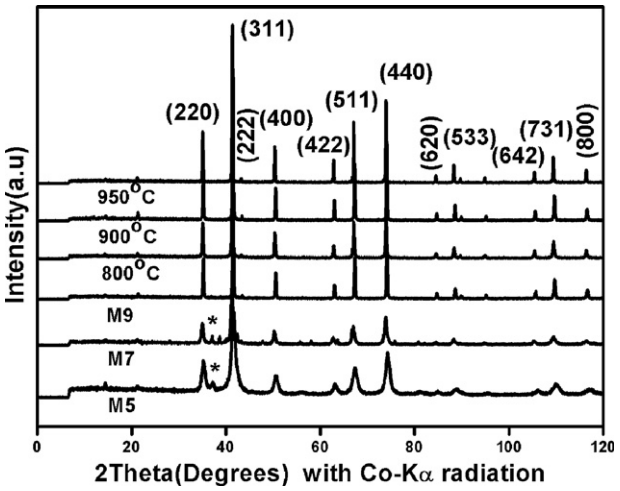

Fig. 1. XRD patterns for the annealed (M5, M7 and M9) and sintered samples (800 °C, 900 °C and 950 °C).

polycrystalline MgCuZn ferrite. It is also observed that the diffraction peaks became sharper, narrower along with increased intensity with increased annealing temperature. This can be attributed to the improvement in both the crystallite size and crystallinity as a function of annealing temperature. Barati [12] observed a similar type of structural behaviour as a function of annealing temperature. The mean crystallite sizes were calculated from X-ray line broadening of the (3 1 1) diffraction peak using Debye Scherrer's equation by taking in to account the instrumental line broadening factor [15].

$$D_{xrd} = \frac{0.9 \times \lambda}{\beta \cos\theta}$$

where λ is the wavelength of the X-rays (1.78897 Å), $\beta = \sqrt{\beta_{meas}^2 - \beta_o^2}$ is the full width at half maximum (in radians) after correcting the instrumental broadening factor (β_o), β_{meas} is the observed full width at half maximum and θ is the Bragg's angle. Since the crystallite size showed an increasing trend as a function of annealing temperature which implies there is progressive growth of crystallites. The lattice parameter calculations for the samples M5 and M7 are excluded due to the presence of secondary phase. The lattice constant (a) of the sample M9 is determined using Nelson–Riley (NR) extrapolation method by minimizing both the systematic and random error. The values of the lattice parameter obtained from each reflected plane were plotted against the Nelson–Riley function $F(\theta)$ (NR). A straight line graph with a positive intercept was obtained [16].

$$F(\theta) = \frac{1}{2}\left[\frac{\cos^2\theta}{\sin\theta} + \frac{\cos^2\theta}{\theta}\right]$$

The extrapolation of the straight line to $F(\theta) = 0$ or $\theta = 90^\circ$ gives the accurate lattice constant. The structural and magnetic parameters as a function of annealing temperature are presented in Table 1.

The XRD patterns (Fig. 1) for the samples sintered at three different temperatures showed pure spinel phase with no other secondary phase. Thus in the process of sintering, a small amount of secondary phase (Fe_2O_3) which was seen in the powder sample M5 was reacted by reactive sintering and it got transformed into crystalline pure spinel MgCuZn ferrite [17]. The lattice constant (a) is almost same for the three sintered samples. The observed lattice constant values are in good agreement with the reported results [13]. The crystallite size for all the samples along with the lattice constant is shown in Table 2.

Table 1
Structural and magnetic parameters for the annealed samples.

Annealed samples	M5	M7	M9
Crystallite size (nm)	9	21	52
Grain size (nm)	<10	30	87
Lattice constant (Å)	–	–	8.4089
Saturation magnetisation M_s (emu/g)	31.23	35.66	47.68
Coercivity H_c (Oe)	2	23.09	14.36
Remnant magnetisation M_r (emu/g)	0.2	2.36	4.128
Remanence ratio $R = M_r/M_s$	0.0064	0.0066	0.0865

Table 2
Structural and magnetic parameters for the sintered samples.

Sintering temperature	800 °C	900 °C	950 °C
Lattice constant (Å)	8.4168	8.4114	8.4161
Crystallite size (nm)	42	53	74
Grain size (nm)	73	139	270
Static permeability μ_i at 1 MHz	12	41	75
Cut-off frequency (MHz)	32	30.8	30.4

3.2. Fourier transform infrared spectroscopy analysis (FTIR)

Chemical and structural changes that take place during the heat treatment can be monitored by a spectroscopic analysis. Fig. 2 shows IR spectra of the annealed samples (M5, M7 and M9). The samples show weak bands at about 3400, 1600,

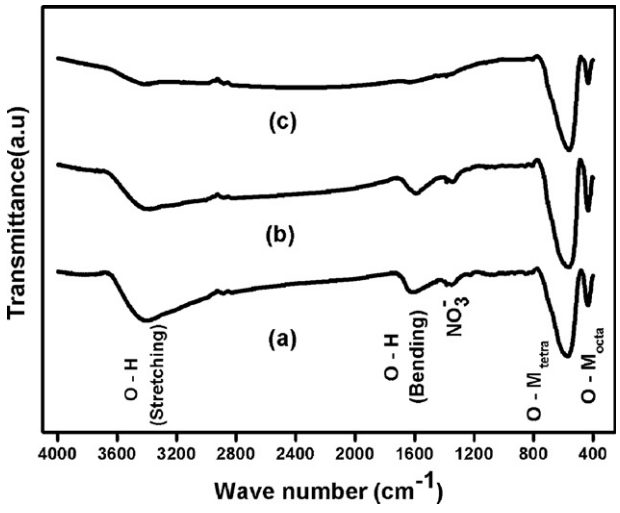

Fig. 2. FTIR spectra for the annealed samples M5 (a), M7 (b) and M9 (c).

1384 cm^{-1} .The first band around 3400 cm^{-1} corresponds to the stretching mode of O–H group in the free and absorbed water and PVA. The second band around 1600 cm^{-1} belongs to H–O–H bending vibration of the residual water .The third one around 1384 cm^{-1} is attributed to the anti-symmetric NO_3^{-1} stretching vibration [18]. In addition to that there is a low intensity frequency band around 2900 cm^{-1} corresponding to the stretching vibration of CH_2 implies the presence of PVA [19].The intensity of these bands reduces as a function of annealing temperature indicating the formation of pure spinel ferrite. Thus, FTIR analysis throw a light on annealing temperature required for the completion of solid state reaction by removing the unwanted species or ions present in the material. The presence of these ions will deteriorate material properties. Besides that there are two strong frequency bands (ν_1, ν_2) which were observed in all the samples at 571 and 434 cm^{-1} corresponding to characteristics of ferrites. The band ν_1 is assigned to the vibration of the bond between the oxygen ion and the tetrahedral metal ion O–M_{tetra} and the band ν_2 is assigned to the vibration of the bond between the oxygen ion and the octahedral metal ion O–M_{octa} [20]. The difference in band positions is due to change in bond length of Fe^{3+}–O^{2-} at tetrahedral (0.189 nm) and octahedral (0.199 nm) sites respectively [21]. It is observed that there is no shift in the frequency band ν_1 for the samples M5 and M7 where as for the sample M9 there was a shift in frequency band. The slight variation in ν_1 is due to change in microstructure with increased annealing temperature. The frequency band ν_2 remains at the same position for the three annealed samples.

3.3. Micro structural and EDS analysis

It is well known that the magnetic properties of a material are sensitive to its microstructure. FESEM micrographs for the annealed samples M5, M7 and M9 are shown in Fig. 3(a)–(c) respectively. It is inferred from the micrographs that in the case of sample M5, the grains have spherical shape with ultra fine size and they are at the formation stage. Since the grains are of very small size (<10 nm) it is difficult to calculate the average grain size in this case. The mean grain size for the samples M7 and M9 with standard deviation was obtained by counting large number of grains to ensure accurate measurement. The sample M7 and M9 showed polyhedral grains with increased grain size compared to the sample M5. The sample M7 displayed a homogeneous microstructure with narrow grain size distribution having an average grain size of 30 nm whereas for the sample M9 an average size is of 87 nm. The grain sizes for the present samples were higher than the crystallite size (D_{xrd}) obtained using Debye Scherrer's formula from XRD, indicating that the crystallites are agglomerated to form grains. The crystallite size and grain size showed almost linear increase with increasing annealing temperature. The morphology of the annealed samples gets transformed from spherical to polyhedral shape with increasing annealing temperature. This is due to the replacement of solid–vapour surface of the crystals by solid–solid interface via solid state diffusion, in order to, reduce overall surface energy [22]. The chemical composition of the annealed samples was also investigated using EDS spectral analysis. The qualitative elemental analysis obtained from EDS

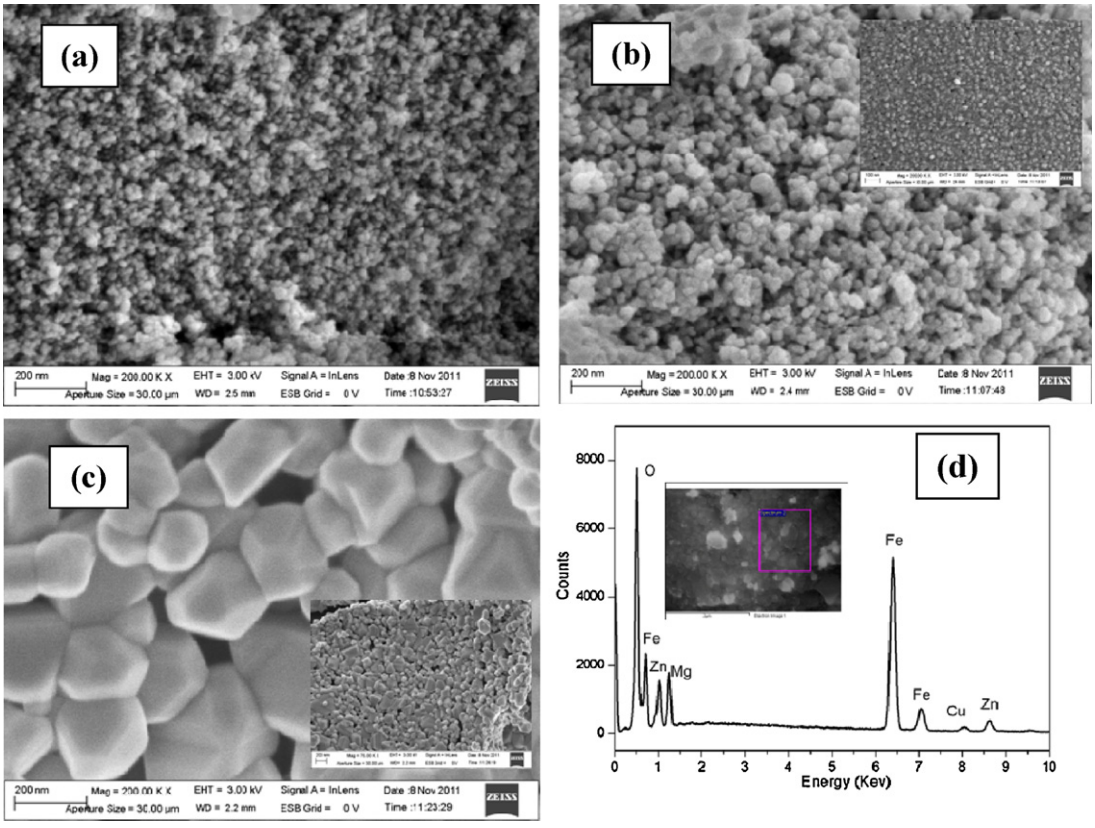

Fig. 3. FESEM microstructures for the annealed samples M5 (a), M7 (b) and M9 (c) and EDS spectra for the sample annealed at 900 °C (d).

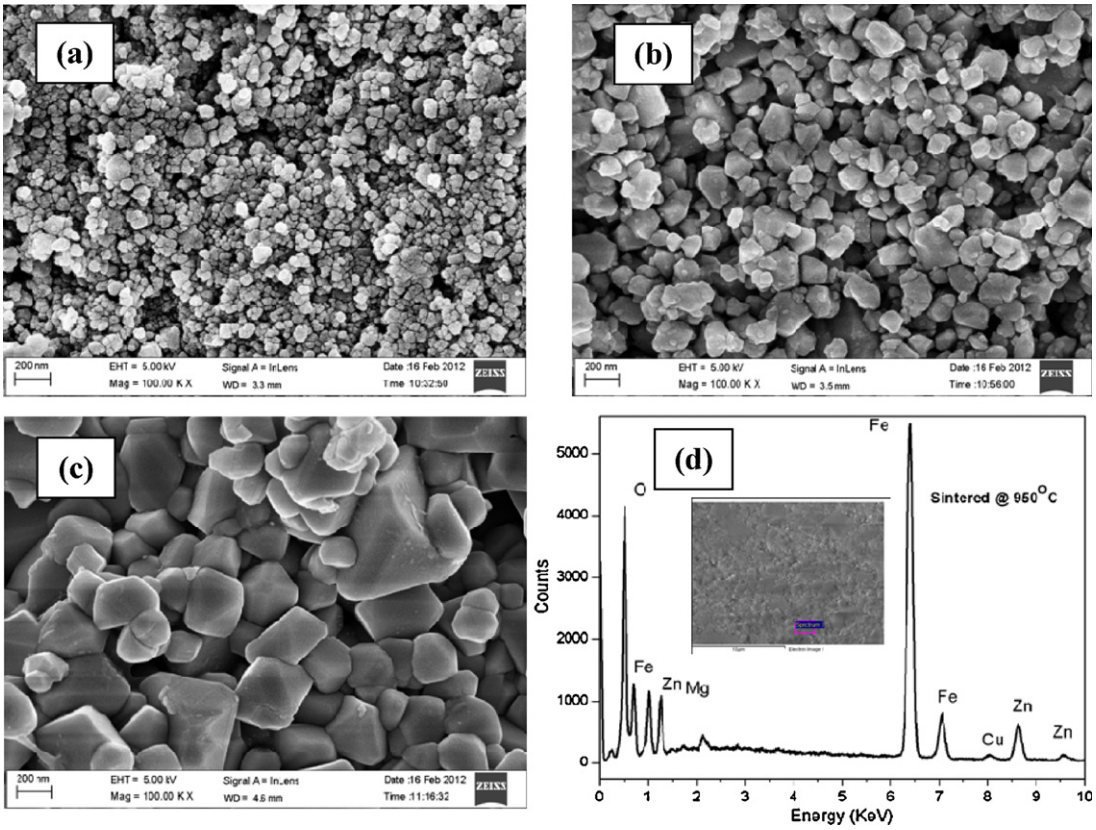

Fig. 4. FESEM microstructures for the sintered samples 800 °C (a), 900 °C (b), 950 °C (c) and EDS spectra for the sample sintered at 950 °C (d).

spectra showed peaks corresponding to the elements Mg, Cu, Zn, Fe and O. The samples M5 and M7 showed non homogeneous chemical composition, due to the presence of small trace of secondary phase (Fe_2O_3) whereas the sample M9 exhibited the chemical composition similar to the proposed stoichiometric formula. For instance, the EDS spectra for the sample M9 at a particular location is as shown in Fig. 3(d).

The FESEM micrographs for the sintered samples are as shown in Fig. 4. The sample sintered at 800 °C contains spherical grains with narrow grain size distribution having an average grain size of 73 nm with standard deviation of 3 nm. Fig. 4(b) illustrates the microstructure of the sample sintered at 900 °C, comprising polyhedral grains with improved grain size and there is an improved intact among the grains compared to the sample sintered at 800 °C. The average grain size for this sample is 139 nm with standard deviation of 3.7 nm. The sample sintered at 950 °C presented a microstructure with smooth and clean octahedral shaped grains with nearly uniform diameter. The grains have an average diameter of 270 nm with standard deviation of 13 nm. All the samples exhibited a relatively uniform grain size distribution which was assessed from the values of standard deviation. It is well established that densification of ferrites is carried out by diffusion of atoms through the grain boundary; grain growth by grain boundary migration [23]. In the present case, with increasing sintering temperature, there is an improved densification as well as the grain growth. It is observed that with increasing sintering temperature porosity was reduced. The obtained microstructure of the present samples is useful for attaining good electromagnetic properties like permeability and magnetization. The qualitative and quantitative elemental analysis was carried out on the sintered samples, at a particular location, for examining the formation of stoichiometric MgCuZn ferrite. Fig. 4(d) shows EDS spectra of the sample sintered at 950 °C.

3.4. Room temperature magnetic properties analysis

Fig. 5 represents isothermal magnetization curves at room temperature in an applied magnetic field of 15 kOe for the

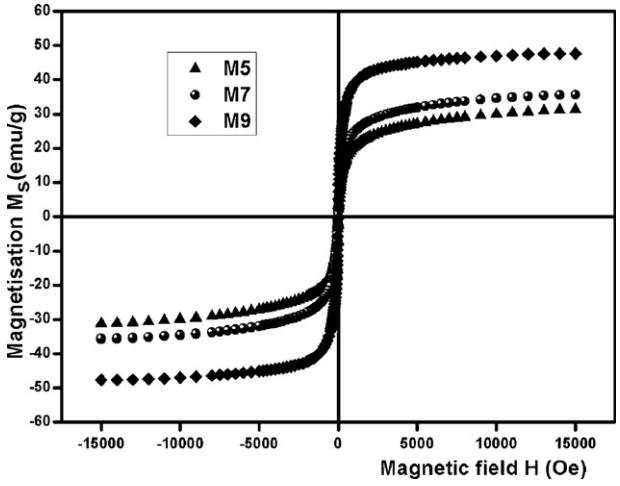

Fig. 5. Room temperature hysteresis loops for the annealed samples M5, M7 and M9.

samples M5, M7 and M9. The samples showed narrow hysteresis loops with low coercivity implied reduced hysteresis losses in the present samples. The magnetic parameters such as saturation magnetisation (M_s), remanent magnetisation (M_r) and coercivity (H_c) (Table 2) were obtained from the hysteresis loop (M−H loop) and these parameters showed dependence on microstructure. The samples M5 and M7 showed non saturating magnetization behaviour even up to an applied magnetic field of 15 kOe indicating the presence of superparamagnetic (SPM) particles in the samples, since the high field curvature of magnetization is due to small particles [24]. It is well known that the saturation magnetization can be tuned both by intrinsic and extrinsic parameters like composition and grain size respectively. The saturation magnetization (M_s) showed increasing trend with annealing temperature. This is because of two reasons. Reduced antiferromagnetic α-Fe_2O_3 content (clearly seen in XRD patterns) with annealing temperature is one of the reasons [25]. The other reason being increased crystallite size with annealing temperature resulting in the formation of multi domain particles, since multi domain particles require low switching field for domain wall motion thereby improving saturation magnetisation [26]. The coercivity (H_c) in general is a measure of magnetization reversal process under the action of an applied field. It depends mainly on particle size and crystalline anisotropy constant [27]. The coercivity showed an increasing trend with increasing annealing temperature up to 700 °C and then decreases in case of sample annealed at 900 °C. This can be attributed to variations in particle size with annealing temperature. The sample M5 exhibited insignificant coercivity ($H_c \sim 2$ Oe) validating the SPM nature. When the particle size is more than the critical diameter (D_c) for single domain then the coercivity can be determined from domain wall displacement. When the particle size is in the order of D_c, the coercivity is determined from domain rotation [28]. The critical diameter for single domain particle is [29]

$$D_c = \frac{9w_p}{2\pi M_s^2}$$

where w_p is the domain wall energy and is given by $w_p = (2k_BT_CK_V/a)^{1/2}$, M_s is saturation magnetisation, k_B is Boltzmann constant, T_c is Curie temperature, K_V is magnetocrystalline anisotropy constant and a is the lattice constant.

The anisotropy constant (K_1), Curie temperature (T_c) and saturation magnetisation values were assumed from the literature reports close to the present composition and the values are $K_1 = -2.2 \times 10^4$ erg/cm^3 [30], $T_c = 132$ °C [30] and $M_s = 235$ Gauss [6]. The observed lattice constant is 8.4168 Å. Thus the critical diameter obtained from the above formula is 44 nm.

In the present case, the sample annealed above 700 °C has the particle size (52 nm) which is more than the critical size for single domain and hence the sample M9 exists in multi domain state. Thus transition from single domain to multi domain state took place with increased annealing temperature. The remanence ratio $R = M_r/M_s$ is referred to as squareness of a hysteresis loop and is dependent on anisotropy constant and particle diameter [31]. This ratio is observed to be increasing with increase of annealing temperature which corresponds to increase in particle size [32] and this is in good agreement with both XRD and FESEM results. The variation of saturation magnetisation and coercivity as a function annealing temperature is represented in Fig. 6.

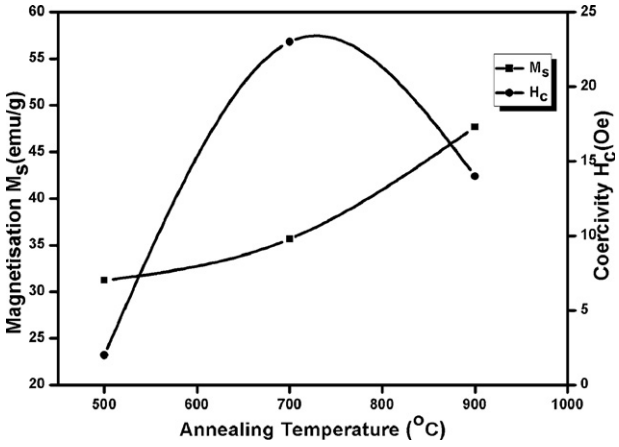

Fig. 6. Variation of saturation magnetisation and coercivity with annealing temperature.

3.5. Frequency dispersion of permeability spectra analysis

Frequency dispersion of permeability for the samples sintered at 800 °C, 900 °C and 950 °C are as shown in Fig. 7. The basic magnetization processes contributing to permeability are spin rotation; domain wall bulging; domain wall displacement [33]. In low frequency region, both domain wall (DW) bulging and displacement affect the permeability. DW bulging gives rise to frequency dispersion of permeability related to relaxation type and it is a reversible process. The relaxation frequency is proportional to the extent of pinning [34]. The DW displacement is of resonance type and its frequency increases as the size of the DW reduces [35]. The

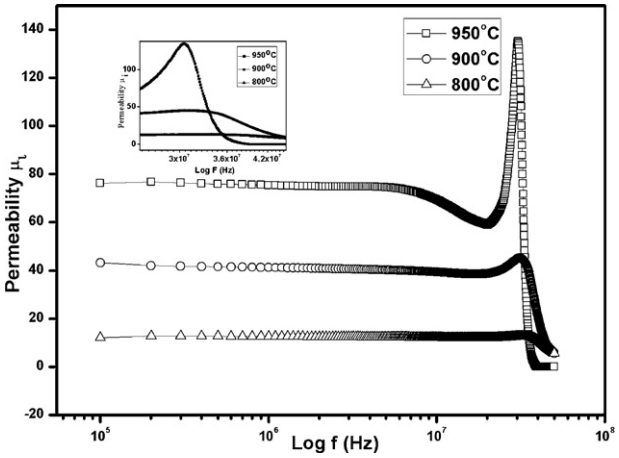

Fig. 7. Frequency dispersion of permeability for the sintered samples 800 °C (a), 900 °C (b) and 950 °C. The inset shows high frequency dispersion of permeability.

DW displacement contribution to the permeability can be improved if the measurement is carried out in DC magnetic field. As the applied DC magnetic field increases, at one particular filed called propagation field the domain walls are unpinned and start to displace [36]. The DW displacement is an irreversible process and it is related to hysteresis losses in M−H loops. The spin rotation occurs at high frequency range (GHz) in case of single domain particles since the entire spins in the domain has to rotate in the applied field direction.

Frequency dispersion of permeability for the present samples shows decrease of permeability at low frequency and has maximum at higher frequency followed by a drop in the permeability. The high frequency dispersion of permeability is represented in the inset of Fig. 7. This is attributed to the mixed behaviour of the type relaxation resonance phenomenon. Herrera [34] observed similar type of frequency dispersion of permeability in V_2O_5 doped $Ni_{0.7}Zn_{0.3}Fe_2O_4$ ferrite system. According to the CPS (complex permeability spectra) model proposed by Jankovskis [35] considering both the grain size and standard deviation parameters showed occurrence of domain wall resonance at higher frequency, due to intragranular defects. It is already discussed earlier that the grain size increased with sintering temperature indicating the presence of domain walls and hence exhibited similar type of resonance behaviour as discussed above. Yue et al. [11] also pointed out the similar type of performance with applied ac filed in Cu substituted MgZn ferrites. It is well known that domain wall permeability is dominant in low frequency region. The permeability showed an increasing trend with sintering temperature due to increased grain size. The static permeability μ_i at 1 MHz for the samples sintered at 800 °C, 900 °C and 950 °C is 12, 41 and 75, respectively. The cut-off frequency exhibited decreasing trend with increasing sintering temperature. Thus the present samples are obeying Snoek's law. The cut-off frequency for the samples sintered at 800 °C, 900 °C and 950 °C is 32, 30.8 and 30.4 MHz respectively. The observed cut-off frequency is high compared to the reported values of MgCuZn ferrite systems [11–14]. The samples sintered at 800 °C and 900 °C exhibited flat profile of permeability with frequency up to 20 MHz, indicating compositional stability and quality of the material. For the sample sintered at 950 °C, dispersion in permeability increased, having frequency stability up to 6.4 MHz only. Thus the cut off frequency can be tuned based on our requirement by changing the heat treatment conditions.

4. Conclusions

MgCuZn nanoparticles were prepared through sol–gel method using PVA as a chelating agent. The structural and magnetic properties with respect to both annealing and sintering heat treatment conditions were studied and the results are summarized as follows:

1. The formation of MgCuZn nano ferrite takes place at low annealing temperature of 500 °C. It is observed that both the crystallite size and saturation magnetisation improved with increased annealing temperature.
2. The variations of magnetic properties with annealing temperature demonstrated transition from single domain to multi domain state and the critical diameter for single domain particle is 44 nm.
3. The static permeability improved as a function of sintering temperature and it is in accordance with the grain size.
4. The samples exhibited good frequency stability up to 20 MHz frequency range. The cut-off frequency for the samples sintered at 800 °C, 900 °C and 950 °C is 32 MHz, 30.8 MHz and 30.4 MHz, respectively.

Acknowledgements

Authors wish to thank Prof. C. Bansal, Dean, School of Physics, University of Hyderabad (UOH) for providing XRD and FESEM facility. Also, the authors would like to express their gratitude to Dr. G. Jagan Reddy and Dr. A.R. James, DMRL, Hyderabad; Dr. P. Sarah, Vardaman Engineering College, Hyderabad for providing magnetic measurements.

References

[1] E. Manova, B. Kunev, D. Paneva, I. Mitov, L. Petrov, Mechano-synthesis, characterization, and magnetic properties of nanoparticles of cobalt ferrite, $CoFe_2O_4$, Chemistry of Materials (2004) 5689–5696.
[2] T. Tsutaoka, T. Kasagi, K. Hatakeyama, Magnetic field effect on the complex permeability for a Mn–Zn ferrite and its composite materials, Journal of the European Ceramic Society 19 (1999) 1531–1535.
[3] A. Daigle, J. Modest, A.L. Geiler, S. Gillette, Y. Chen, M. Geiler, B. Hu, S. Kim, K. Stopher, C. Vittoria, V.G. Harris, Structure, morphology and magnetic properties of $Mg_{(x)}Zn_{(1-x)}Fe_2O_4$ ferrites prepared by polyol and aqueous co-precipitation methods: a low-toxicity alternative to $Ni_{(x)}Zn_{(1-x)}Fe_2O_4$ ferrite, Nanotechnology 22 (2011) 305708.
[4] S.A. Ghodake, U.R. Ghodake, S.R. Sawant, S.S. Suryavanshi, P.P. Bakare, Magnetic properties of NiCuZn ferrites synthesized by oxalate precursor method, Journal of Magnetism and Magnetic Materials 305 (2006) 110–119.
[5] M. Yan, J. Hu, W. Luo, W.Y. Zhang, Preparation and investigation of low firing temperature NiCuZn ferrites with high relative initial permeability, Journal of Magnetism and Magnetic Materials 303 (2006) 249–255.
[6] H. Su, H. Zhang, X. Tang, B. Liu, Z. Zhong, Study on low-temperature sintered NiCuZn and MgCuZn spinel ferrites, Journal of Alloys and Compounds 475 (2009) 683–685.
[7] X. Qi, J. Zhou, Z. Yue, Z. Gui, L. Li, Effect of Mn substitution on the magnetic properties of MgCuZn ferrites, Journal of Magnetism and Magnetic Materials 251 (2002) 316–322.
[8] M. Penchal Reddy, W. Madhuri, M. Venkata Ramana, N. Ramamanohar Reddy, K.V. Siva Kumar, V.R.K. Murthy, K. Siva Kumar, R. Ramakrishna Reddy, Effect of sintering temperature on structural and magnetic properties of NiCuZn and MgCuZn ferrites, Journal of Magnetism and Magnetic Materials 322 (2010) 2819–2823.
[9] V.D. Kassabova-Zhetcheva, L.P. Pavlova, B.I. Samuneva, Z.P. Herkezova-Zheleva, I.G. Mitov, M.T. Mikhov, Characterization of superparamagnetic $Mg_xZn_{1-x}Fe_2O_4$ powders, CEJC 5 (2007) 107–117.
[10] B.K. Nath, P.K. Chakrabarti, S. Das, U. Kumar, P.K. Mukhopadhyay, D. Das, Mossbauer studies on nanoparticles of zinc substituted magnesium ferrite, Journal of Surface Science Technology 21 (2005) 169–182.
[11] Z. Yue, J. Zhou, L. Li, X. Wang, Z. Gui, Effect of copper on the electromagnetic properties of Mg–Zn–Cu ferrites prepared by sol–gel auto-combustion method, Materials Science and Engineering B 86 (2001) 64–69.
[12] M.R. Barati, Influence of zinc substitution on magnetic and electrical properties of MgCuZn ferrite nanocrystalline powders prepared by sol–gel

auto-combustion method, Journal of Alloys and Compounds 478 (2009) 375–380.
[13] M. Manjurul Haquea, M. Huqa, M.A. Hakim, Densification, magnetic and dielectric behaviour of Cu-substituted Mg–Zn ferrites, Materials Chemistry and Physics 112 (2008) 580–586.
[14] J. Murbe, J. Topfer, Mg–Cu–Zn ferrites for multilayer inductors, International Journal of Applied Ceramic Technology 4 (2007) 415–422.
[15] K. Venkateswarlu, A. Chandra Bose, N. Rameshbabu, X-ray peak broadening studies of nanocrystalline hydroxyapatite by Williamson–Hall analysis, Physica B 405 (2010) 4256–4261.
[16] C. Sujatha, K. Venugopal Reddy, K. Sowri Babu, A. RamaChandra Reddy, K.H. Rao, Structural and magnetic properties of Mg substituted NiCuZn nano ferrites, Physica B 407 (2012) 1232–1237.
[17] A.C.F.M. Costa, M.R. Morelli, R.H.G.A. Kiminami, Microstructure and magnetic properties of $Ni_{1-x}Zn_xFe_2O_4$ synthesized by combustion reaction, Journal of Materials Science 42 (2007) 779–783.
[18] S. Yan, J. Geng, L. Yin, E. Zhou, Preparation of nanocrystalline NiZnCu ferrite particles by sol–gel method and their magnetic properties, Journal of Magnetism and Magnetic Materials 277 (2004) 84–89.
[19] S.J. Kim, S.J. Park, S.I. Kim, Swelling behaviour of interpenetrating polymer network hydrogels composed of poly(vinyl alcohol), Reactive & Functional Polymers 55 (2003) 29–53.
[20] J. Jacob, M. Abdul Khadar, Investigation of mixed spinel structure of nanostructured nickel ferrite, Journal of Applied Physics 107 (2010) 114310.
[21] K.B. Modi, U.N. Trivedi, P.U. Sharma, V.K. Lakhani, M.C. Chhantbar, H.H. Joshi, Study of elastic properties of fine particle copper–zinc ferrites through infrared spectroscopy, Indian Journal of Pure & Applied Physics 44 (2004) 165–168.
[22] C.H. Chia, S. Zakaria, M. Yusoff, S.C. Goh, C.Y. Haw, S. Ahmadi, N.M. Huang, H.N. Lim, Size and crystallinity-dependent magnetic properties of $CoFe_2O_4$ nanocrystals, Ceramics International 36 (2010) 605–609.
[23] H. Su, X. Tang, H. Zhang, Z. Zhong, J. Shen, Sintering dense NiZn ferrite by two-step sintering process, Journal of Applied Physics 109 (2011) 07A501.
[24] V. Franco, A. Conde, Influence of anisotropy on the grain size distribution derived from superparamagnetic magnetization curves, Journal of Magnetism and Magnetic Materials 277 (2004) 181–186.
[25] R. Gimenes, M.R. Baldissera, M.R.A. da Silva, C.A. da Silveira, D.A.W. Soares, L.A. Perazolli, M.R. da Silva, M.A. Zaghete, Structural and magnetic characterization of $Mn_xZn_{1-x}Fe_2O_4$ ($x = 0.2$; 0.35; 0.65; 0.8; 1.0) ferrites obtained by the citrate precursor method, Ceramics International 38 (2012) 741–746.
[26] E. Girgis, M.M.S. Wahsh, A.G.M. Othman, L. Bandhu, K.V. Rao, Synthesis, magnetic and optical properties of core/shell $Co_{1-x}Zn_xFe_2O_4/SiO_2$ nanoparticles, Nanoscale Research Letters 6 (2011) 460.
[27] A. Ashrafizadeha, A. Ghasemi, A. Paesano Jr., C. Fabiana Cerqueira, M. Xiaoxi Liua, A. Morisakoa, Structural and magnetic properties of $Cu_xMg_{0.5-x}Zn_{0.5}Fe_2O_4$ ($x = 0$–0.5) particles, Journal of Alloys and Compounds 506 (2010) 279–284.
[28] L. Zhao, H. Zhang, Y. Xing, S. Song, S. Yu, W. Shi, X. Guo, J. Yang, Y. Lei, F. Cao, Studies on the magnetism of cobalt ferrite nanocrystals synthesized by hydrothermal method, Journal of Solid State Chemistry 181 (2008) 245–252.
[29] C. Caizer, M. Stefanescu, Nanocrystallite size effect on σ_s and H_c in nanoparticle assemblies, Physica B 327 (2003) 129–134.
[30] D.N. Bhosale, V.M.S. Verenkar, K.S. Rane, P.P. Bakare, S.R. Sawant, Initial permeability studies on Cu–Mg–Zn ferrites, Materials Chemistry and Physics 59 (1999) 57–62.
[31] M.P. Pileni, N. Moumen, J.F. Hochepied, P. Bonville, P. Veillet, Control of the size of cobalt ferrite nanoparticles: synthesis and properties, Journal de Physique 7 (1997), Colloque C1, Supplement au Journal de Physique III de mars (1997) C1 505–508.
[32] H.M.I. Abdallah, T. Moyo, J.Z. Msomi, The effect of annealing temperature on the magnetic properties of $Mn_xCo_{1-x}Fe_2O_4$ ferrites nanoparticles, Journal of Superconductivity and Novel Magnetism 10 (2011), http://dx.doi.org/10.1007/s10948-011-1231-4.
[33] R. Valenzuela, H. Montiel, M.P. Gutierrez, I. Betancourt, Characterization of soft ferromagnetic materials by inductance spectroscopy and magnetoimpedance, Journal of Magnetism and Magnetic Materials 294 (2005) 239–244.
[34] G. Herrera, Domain wall dispersions: Relaxation and resonance in Ni–Zn ferrite doped with V_2O_5, Journal of Applied Physics 108 (2010) 103901.
[35] J. Jankovskis, Presentation of complex permeability spectra of polycrystalline ferrites based on grain size distribution, Journal of Magnetism and Magnetic Materials 272–276 (2004) e1847–e1849.
[36] K.L. Garcia, R. Valenzuela, Domain wall pinning, bulging and displacement in circumferential domains in CoFeBSi amorphous wires, Journal of Applied Physics 87 (2000) 5257–5259.